

STRAY-LIGHT EFFECT ON MAGNETOGRAPH OBSERVATIONS

JONGCHUL CHAE¹, HONG SIK YUN², TAKASHI SAKURAI³ and
KIYOSHI ICHIMOTO³

¹*Big Bear Solar Observatory, New Jersey Institute of Technology, 40386 North Shore Lane,
Big Bear City, CA 92314, U.S.A.*

²*Department of Astronomy, Seoul National University, Seoul 151-742, Korea*

³*National Astronomical Observatory, Mitaka, Tokyo 181, Japan*

(Received 19 June 1997; accepted 3 August 1998)

Abstract. To examine the stray-light effect in magnetograph observations, we have determined the point spread functions of the vector magnetograph mounted on the Japanese Solar Flare Telescope based on two indirect methods, one analyzing the solar limb intensity profile, and the other using the Fourier power spectra of photospheric intensity distributions. Point spread functions consist of two parts: a blurring part which describes seeing and small-spread-angle stray light, and a scattering part which describes large-spread-angle stray light. The FWHM spatial resolution is typically $3.0''$, and the amount of scattered light is about 15% on clear days. We find that the blurring part is well described by a Moffat function whose Fourier transform is given by an exponential function. Our results indicate that polarization measurements of low-intensity magnetic elements like sunspots may be significantly underestimated due to the large-spread-angle stray light, and polarization measurements of magnetic elements which are smaller than $5-7''$ appear to be disturbed by small-spread-angle stray light.

1. Introduction

One of the difficulties often encountered in solar observations is the disturbance due to stray light produced by observing instruments and the Earth's atmosphere. Generally, stray light degrades spatial resolution, reduces intensity contrast, and causes a systematic error in the measurement of light intensity, especially in low-intensity regions like sunspots. A number of studies on the stray light problem have been done in relation to the determination of sunspot intensity (Kneer and Mattig, 1968; Rossbach and Schröter, 1970; Maltby, 1971; Brahde, 1972; Mykland, 1973; Martínez Pillet, 1992), solar limb darkening (Pierce and Slaughter, 1977; Brown, 1982; Toner and Jefferies, 1993), facular contrast (Lawrence *et al.*, 1985) and solar Doppler measurements (Albregtsen and Andersen, 1985; Andersen, 1986).

Magnetograph observations are also affected by stray light (Lites *et al.*, 1991; Keller, 1991). In some of the spectrometer-based magnetograph observations (Lites *et al.*, 1993, 1994) it has been assumed that only the Stokes I parameter is affected by stray light, and the effect of stray light on the measurement of magnetic fields has been taken into account by introducing a free parameter which is determined in the process of model fitting of the Stokes profiles. In high-resolution



filter-based magnetograph observations, small-spread-angle stray light caused by atmospheric seeing has been a big problem in determining the true size and magnetic field strength of small magnetic elements. Thus several attempts have been made to overcome the disturbance due to seeing, including image deconvolution (Koutchmy, 1991) and speckle polarimetry (Keller and von der L uhe, 1992). Quite recently, Lee *et al.* (1997) showed that seeing may affect even magnetic flux measurements because a part of the polarization signal is spread out to below the detection limit. The stray-light effect on magnetograph observations appears to be more serious than that on photometry. For example, a filter-based videomagnetograph, one of the popular types of magnetographs, usually integrates a number of frames to increase sensitivity. Therefore, magnetograms may be subject to image motion during integration, resulting in poorer spatial resolution than a short-exposure image taken under the same atmospheric condition. In addition, because of the relatively complex optical parts such as the birefringent filter and polarizer, it is likely that more instrumental stray light is produced in magnetograph observations than in white-light observations. The stray-light effect on the measurements of polarization is rather complicated because the observed degree of polarization is a nonlinear function of the Stokes parameters which may be affected by stray light.

In the present paper, we investigate systematically how stray light affects filter-based magnetograph observations. The distribution of stray light over spread angle is mathematically described by a point spread function (PSF) of the observing system. It is well known that determining point spread functions in solar observations is non-trivial because of the absence of point light sources. We resort to two indirect methods to determine the PSF: one using intensity profiles across the limb and the other using power spectra of photospheric intensity fluctuations on the disk. We examine both small-spread-angle stray light originating from seeing, and large-spread-angle stray light originating from the instrument and the Earth's atmosphere.

2. Basic Formulation

Basically, filter-based magnetograph observations produce two-dimensional distributions of integrated Stokes parameters $I(\mathbf{r})$, $Q(\mathbf{r})$, $U(\mathbf{r})$, and $V(\mathbf{r})$, where \mathbf{r} denotes the spatial position on the image plane. The circular polarization is then given by V/I , and the linear polarizations by Q/I and U/I . From now on, we will work only with I and V , since the same formulae used on V can be applied to Q and U . We consider the disturbed Stokes images I^{obs} and V^{obs} which result from spatial re-distributions of disturbance-free Stokes images I and V . Following the conventional approach, we assume that the spatial re-distributions can be described by the convolutions of Stokes images by a point spread function ψ ,

$$I^{\text{obs}} = I * \psi, \quad (1)$$

$$V^{\text{obs}} = V * \psi , \quad (2)$$

where $*$ is the convolution operator. We found that it is convenient to decompose the intensity, I , into two components: background component $I_{\text{bg}}(\mathbf{r})$ and residual component $I_{\text{re}}(\mathbf{r})$ so that

$$I = I_{\text{bg}} + I_{\text{re}} . \quad (3)$$

The background component is defined by the intensity distribution of the quiet Sun, which is rotationally symmetric about the solar disk center. Then the light re-distribution relation for I is decomposed into two separate equations

$$I_{\text{bg}}^{\text{obs}} = I_{\text{bg}} * \psi , \quad (4)$$

$$I_{\text{re}}^{\text{obs}} = I_{\text{re}} * \psi . \quad (5)$$

We normalize I_{bg} , I_{re} , and V so that I_{bg} is unity at disk center. Following Hansen (1973), the point spread function is also normalized so that $I_{\text{bg}}^{\text{obs}} = I_{\text{bg}} * \psi = 1$ at disk center. For practical purpose, we split the point spread function into two parts: a small-spread-angle part ψ_{bl} , usually called the blurring part, and a large-spread-angle part ψ_{sc} , i.e., the scattering part (cf., Brahde, 1972):

$$\psi = (1 - \epsilon)\psi_{\text{bl}} + \epsilon\psi_{\text{sc}} . \quad (6)$$

Both ψ_{bl} and ψ_{sc} are normalized in the same way as ψ . Thus the new parameter ϵ is equal to the fraction of stray light contributed by the scattering part, and is commonly called the scattered-light fraction. We will see later that this separation into two parts is physically plausible. Since I_{re} and V can be either positive or negative and are close to zero in the field-free or weak-field regions, the convolutions of these images by the large-spread-angle scattering part can be considered to be zero to a good approximation. This results in

$$I_{\text{re}}^{\text{obs}} = (1 - \epsilon)I_{\text{re}} * \psi_{\text{bl}} , \quad (7)$$

$$V^{\text{obs}} = (1 - \epsilon)V * \psi_{\text{bl}} . \quad (8)$$

3. Methods of Point-Spread-Function Determination

3.1. LIMB INTENSITY PROFILE METHOD

If it were not for stray-light disturbance, the solar brightness would abruptly decrease to zero at the limb, since the thickness of the photosphere is far below the typical spatial resolution of long-integration magnetograph observations. In real observations, however, stray light smears the limb edge, and the intensity outside the limb is non-zero. Therefore, the intensity profile across the limb is a good measure of stray-light distribution, and can be used for the determination of the point spread function. The undisturbed limb intensity profile can be described as

$$I_{\text{bg}}(r) = \begin{cases} \phi_{\text{bg}}(r) : r < 1, \\ 0 : r \geq 1, \end{cases} \quad (9)$$

where r is the normalized distance from disk center. The center-to-limb variation of intensity $\phi_{\text{bg}}(r)$ is well described by a polynomial of $\mu = \sqrt{1 - r^2}$ so that

$$\phi_{\text{bg}}(r) = \sum_k c_k \mu^k. \quad (10)$$

Once I_{bg} is specified, the point spread function can be determined by solving the inversion problem defined by Equation (4). We assume that the point spread function is rotationally symmetric about the origin and can be described by a linear combination of a number of Gaussian functions and Lorentzian functions:

$$\psi(r) = \sum_j a_j f_j(r), \quad (11)$$

where $f_j(r)$ is a basis function which we choose to be either a Gaussian function

$$G(r; b_j) \equiv \frac{1}{\pi b_j^2} \exp\left(-\left(\frac{r}{b_j}\right)^2\right) \quad (12)$$

or a Lorentzian function

$$L(r; b_j) \equiv \frac{1}{\pi(b^2 + r^2)}. \quad (13)$$

The width parameters b_j can be freely chosen. It follows from Equation (4) that

$$I_{\text{bg}}^{\text{obs}}(r) = \sum_j a_j \Phi_j(r), \quad (14)$$

where the contribution functions

$$\Phi_j = I_{\text{bg}} * f_j \quad (15)$$

are numerically calculated by using the formula given by Wittman and Wöhl (1975) and Martínez Pillet (1992). Now the determination of the point-spread function has been reduced to the problem of determining a_j from the model fit of limb-intensity profile. Two more free parameters are additionally introduced and determined from the model fit: one for the adjustment of intensity normalization and the other for the adjustment of distance normalization. Introducing these two parameters is necessary because the normalizations made based on observations may be subject to errors which systematically affect the intensity values and distances of all the data points. Particularly determining the limb position from the observations

is not a trivial process because of the atmospheric seeing. Toner and Jefferies (1993) developed a method of determining the limb position from the zeros of the Hankel transform of the observed limb intensity profile, which is insensitive to the seeing. In the present paper, we introduce the parameter for distance normalization, which allows the precise determination of the limb position via the model fit. Model fits have been done by using the nonlinear fitting algorithms of the Levenberg–Marquardt method (Press *et al.*, 1986).

We now describe how to determine the coefficients c_k introduced in Equation (10). We find that a model fit of the disk portion of the observed intensity profile $I_{\text{bg}}^{\text{obs}}$ using Equation (10) yields a good estimate of the coefficients. From the model fit of the whole observed intensity profile using Equation (14), the point spread function ψ is determined. The point-spread function is decomposed into a blurring part $(1 - \epsilon)\psi_{\text{bl}}$ and a scattering part $\epsilon\psi_{\text{sc}}$ and the scattered light fraction ϵ can be estimated from the model fit. Then the scattered light integral defined by

$$S(r) = I_{\text{bg}} * \psi_{\text{sc}} \quad (16)$$

is evaluated and the coefficients c_k are determined again from the model fit of the disk portion of the stray-light-corrected intensity profile

$$I'_{\text{bg}}(r) = \frac{I_{\text{bg}}^{\text{obs}}(r) - \epsilon S(r)}{1 - \epsilon}. \quad (17)$$

Usually, after two or three repetitions of these iterative steps, the coefficients c_k are determined without ambiguity.

3.2. INTENSITY POWER-SPECTRUM METHOD

It is well-known that observed photospheric intensity power spectra are sensitive to seeing and stray light. Thus if we have a good estimate of disturbance-free intensity power spectrum P , the observed intensity power spectra P^{obs} can be used to derive the Fourier modulus of the point spread function. From the Fourier transform of Equation (7), we get

$$P^{\text{obs}}(\mathbf{k}) = (1 - \epsilon)^2 P(\mathbf{k}) \tau_{\text{bl}}^2, \quad (18)$$

where τ_{bl} is the modulus of Fourier transform of ψ_{bl} . If ψ_{bl} is assumed to be rotationally symmetric, the imaginary part of its Fourier transform is equal to zero and the inverse Fourier transform of τ_{bl} becomes ψ_{bl} . Note that the normalization of ψ_{bl} we use leads to $\tau(0) = 1$. In principle, Equation (18) can be used to derive not only τ_{bl} , but also ϵ . But in real situations, determining ϵ from an observed power spectrum may have a big uncertainty, since the measured value is very sensitive to observed power at low frequencies, for which accuracy is limited by the field of view and the way of subtracting background intensity. The main advantage of the

intensity power-spectrum method lies in the fact that it can determine τ_{bl} , and is simple to use.

4. Observation and Data Reduction

The data we use in the present study were obtained from the observations performed with the vector magnetograph mounted on the Solar Flare Telescope at Mitaka, Japan during August 1992. The details of the telescope and the vector magnetograph are described by Sakurai *et al.* (1995). The magnetograph is a video-magnetograph using a birefringent filter. The filter has a bandwidth of $\frac{1}{8}$ Å and is tuned to -80 mÅ off the center of the Fe I line at 6302.5 Å, where both linear and circular polarizations produced by solar magnetic fields become large. Each frame was recorded on a video CCD camera which covers a field of view of $350'' \times 330''$. The CCD is of the interline type and after digitization has an effective pixel size of $0.67''$. A total of 256 video frames (128 frames for each kind of polarized light) were integrated to produce either of the Stokes I , Q , U , and V images. Then the Stokes I and the polarizations Q/I , U/I , and V/I were saved to hard disk with 16-bit accuracy. Dark frames were taken by closing a mechanical shutter in front of the CCD camera and were subtracted from the observed images. Flat field images were taken by inserting calibration optics into the light beam. The calibration optics are specially designed to generate a uniform image of the space near the entrance pupil on the detector plane (Sakurai *et al.*, 1995).

Figure 1 shows the intensity (I) image and the longitudinal magnetogram (V/I) of a small active region located near the south-east limb on 30 August 1992. We obtained the intensity profile across the limb from the intensity image in the following way. First, we determined the center and radius of the disk in the detector pixel coordinates by making use of the position and curvature of the limb. Second, we calculated the normalized distance from the disk center at every pixel position. Finally, the averages of intensity over a series of concentric rings characterized by radii of r_i and widths of Δr_i were taken to represent intensity values at the discrete distances r_i . To obtain a smooth center-to-limb coverage and a good resolution of the limb using a small number of discrete mesh points, the widths Δr_i of the rings were allowed to change with position, having a maximum value of $10''$ at the disk center and a minimum value of $0.1''$ at the limb. The intensity values determined in this way are represented as open circles in Figure 3.

Figure 2 shows the intensity image and longitudinal magnetogram of the active region NOAA 7260 observed near disk center on 18 August 1992. We calculated the power spectra of many small images taken from local regions without sunspots and took the ensemble average of them to reduce noise. For the calculation of the power spectrum in each small image, we first subtracted the low-frequency pattern from the image and then apodized it with a Hanning function. These two processes are known to be helpful in reducing troubles caused by low-frequency

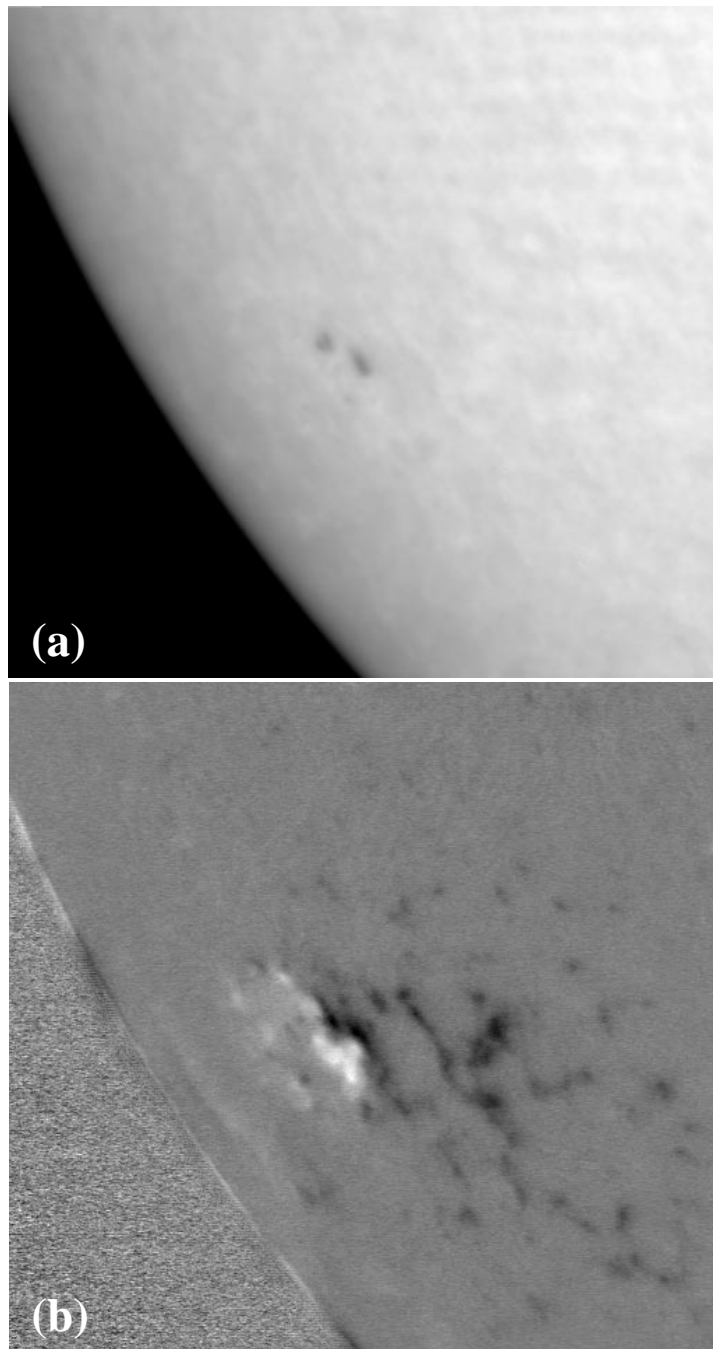


Figure 1. (a) The Stokes I image and (b) the longitudinal magnetogram (V/I) of a small active region observed near the limb on 30 August 1992. The field of view is $350'' \times 330''$.

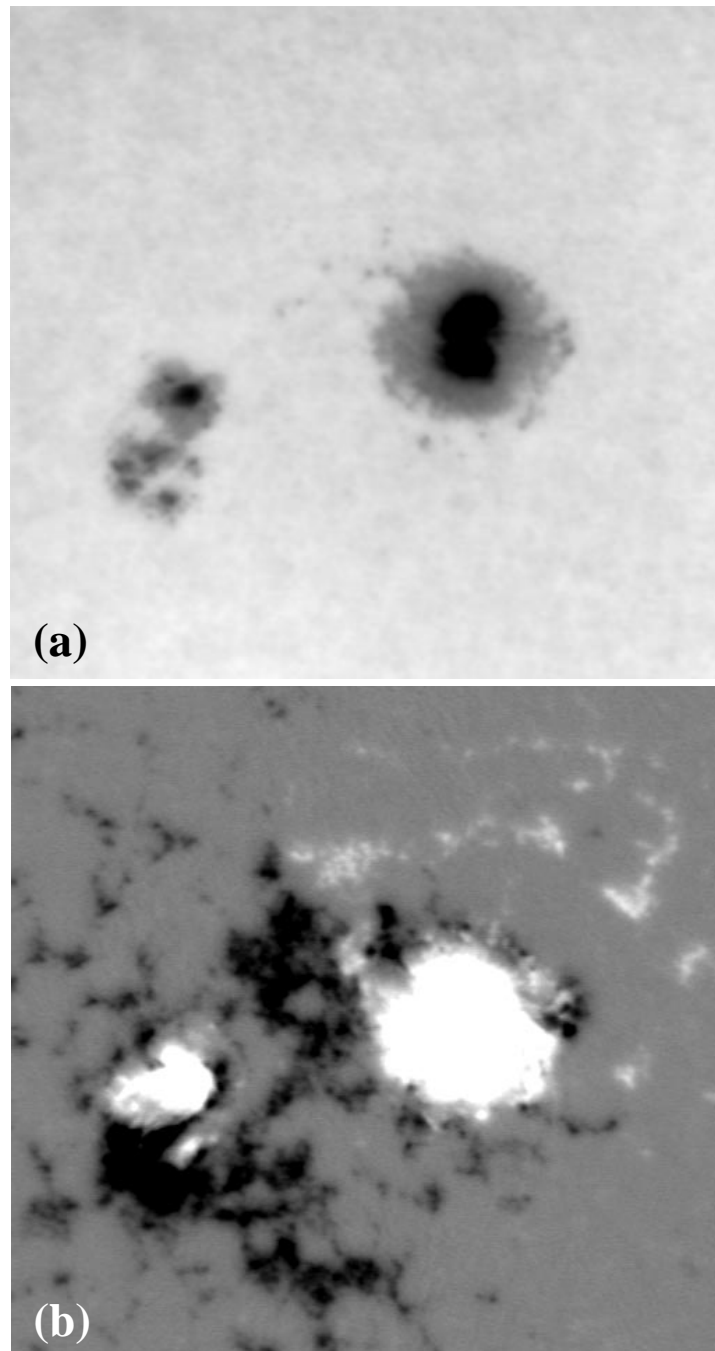


Figure 2. (a) The Stokes I image and (b) the longitudinal magnetogram (V/I) of the active region NOAA 7260 observed near disk center on 18 August 1992. The field of view is $350'' \times 330''$.

spikes and boundary discontinuities (Brault and White, 1971). A two-dimensional power spectrum of the intensity distribution near disk center appears more or less rotationally symmetric so that we took an azimuthal average of the power spectrum.

5. Results

5.1. FROM THE LIMB INTENSITY PROFILE

Figure 3(a) shows the intensity profile across the limb produced from the Stokes I image shown in Figure 1(a) and the result of model fitting. We have found that the center-to-limb variation of undisturbed I is well described by the relation $\phi_{bg} = 0.52 + 0.99\mu - 0.51\mu^2$. We calculated 14 Gaussian contribution functions $\phi_{bg}(r) * G(r; b_j)$ with $b_j = 0.67'', 1.0'', 1.5'', \text{etc.}$, and one Lorentzian contribution function $\phi_{bg}(r) * L(r; b)$ with $b = 100''$. For illustration, we presented in Figure 3(b) some contribution functions which were found to have significant amplitudes from the model fit.

The point-spread function determined from the model fit of the limb-intensity profile is presented in Figure 4. Note that the point-spread function has been determined over a wide range of spread angle from sub-arc sec to larger than $100''$ consistently from the same data presented in Figure 1. We confirm from the figure that the point spread function consists of two distinct parts: the blurring part ψ_{bl} which describes the small-angle light spread, and the scattering part ψ_{sc} which describes the large-angle light spread. The division between small and large spread angles occurs around $30''$. Explicitly speaking, we have

$$(1 - \epsilon)\psi_{bl}(r) = \sum_j a_j G_j(r; b_j) \quad \text{for } b_j = 0.67, 1.5, 2.3, \dots, 30'', \quad (19)$$

and

$$\epsilon\psi_{sc}(r) = aL(r; 100'') + \sum_j a_j G_j(r; b_j) \quad \text{for } b_j = 39, 58, 87, 130''. \quad (20)$$

For comparison, we have presented also King's (1971) stellar profile which was assembled from several different sources. King's profile also has two distinct blurring and scattering parts.

The scattered-light integral defined by $\epsilon S(r)$ is represented by a dotted curve in Figure 3(a). The scattered-light fraction ϵ , which is the amount of scattered light, is about 0.15. The scattered-light integral describes the amount of scattered light as a function of the distance from disk center. Since the function slowly decreases with distance and is not very sensitive to the specific form of either I_{bg} or ψ_{sc} , the same $S(r)$ might be used in observations from different days. Then the spatial distributions of scattered light over the Sun on different days are fully described

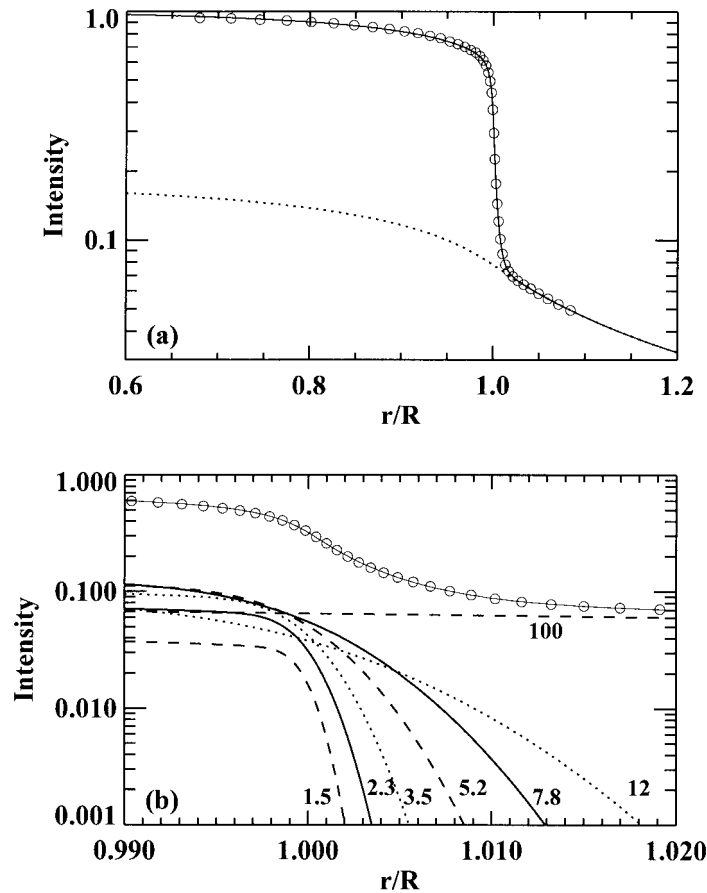


Figure 3. (a) The observed profile of intensity across the limb (open circles). The model fit is drawn as a solid curve, and the scattered-light integral ϵS is presented as a dotted curve. (b) The enlargement of the portion close to the limb. The contribution functions $a_j \Phi_j(r)$ which have $a_j \Phi_j(0)$ greater than 0.05 are shown in the figure, which include 6 Gaussian contribution functions with $b = 1.5, 2.3, 3.5, 5.2, 7.8,$ and $12''$ and 1 Lorentzian function with $b = 100''$.

by the scattered-light fraction ϵ only. We have determined ϵ on different days and found that they range from 0.1 to 0.2 on clear days, and a typical value amounts to 0.15. Even though our results do not allow us to distinguish between scattered light of atmospheric origin and that of instrumental origin, the significant variation from 0.1 to 0.2 indicates that both kinds may be important. Since ϵ is proportional to the observed intensity level at the region far outside the limb, we can also determine ϵ directly from the observed off-limb intensity level without the necessity of model fitting. We found empirically from several days of observations that ϵ is about three times the intensity at $50''$ outside from the limb.

We found that the functional form of the blurring part is different from the traditionally adopted functional forms such as a single Gaussian and Fried's seeing

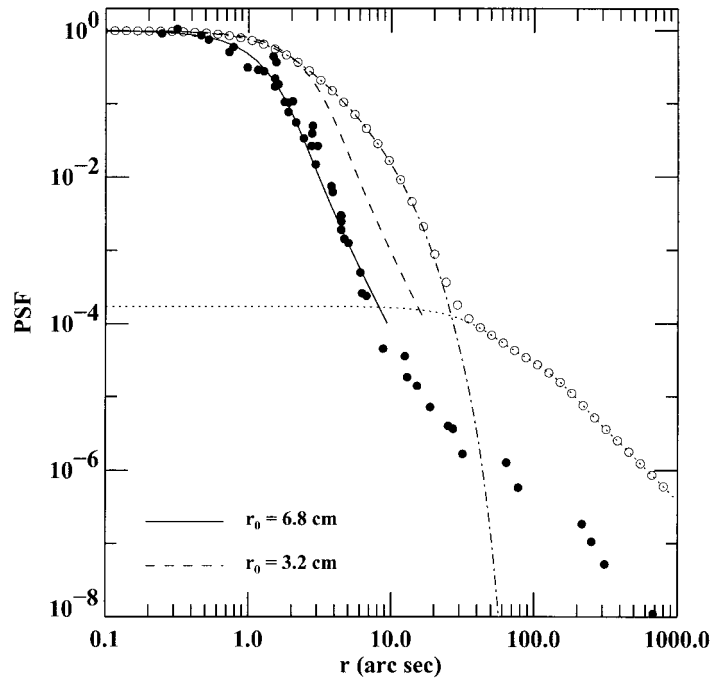


Figure 4. The point-spread function of the magnetograph observation on 30 August 1992 (open circles). It is neatly decomposed into the blurring part (dot-dashed curve) and scattering part (dotted curve). For comparison, King's stellar profile is plotted with closed circles. The solid and dashed curves are Fried's seeing functions which best fit the central part of the point spread functions, respectively.

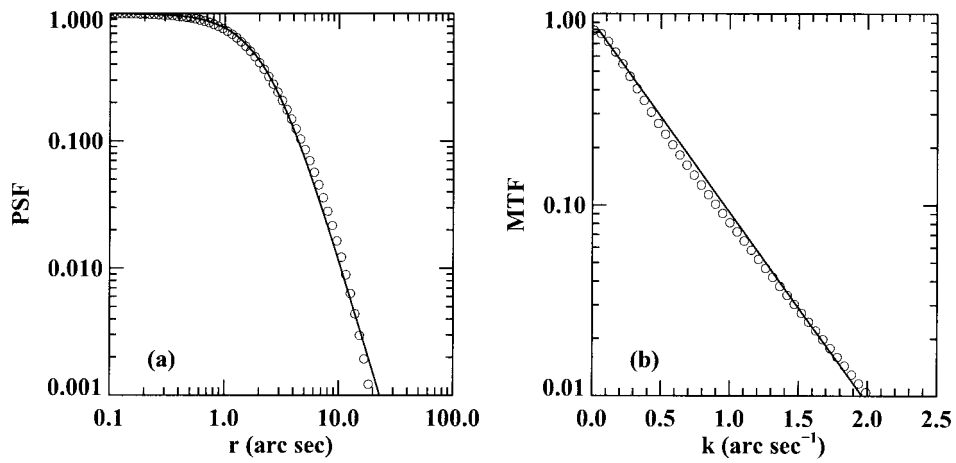


Figure 5. (a) The blurring part of the determined point spread function and (b) its Fourier modulus (modulation transfer function) as indicated by open circles. The solid curves represent the Moffat function and its Fourier transform which best fit the observed ones.

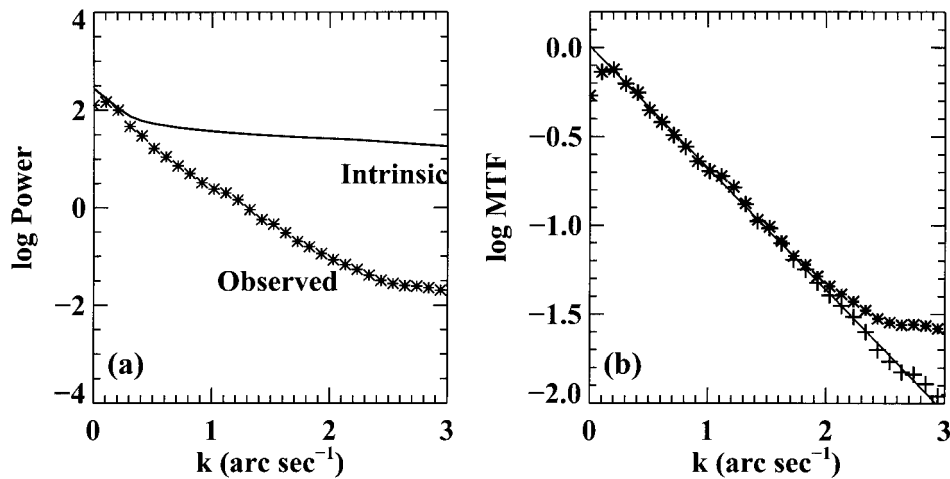


Figure 6. (a) The observed power spectrum compared with the intrinsic power spectrum. (b) The determined MTF without noise correction (*) and with noise correction (+). The solid line is an analytical fit to the estimated MTF.

function (Fried, 1966). We have tried to fit the central parts of our point spread function and King's stellar profile (King, 1971) by Fried's seeing functions whose Fourier transforms are given in the form of $\exp(-(ak)^{5/3})$. The resulting Fried's parameters r_0 are found to be 3.2 cm and 6.8 cm, respectively. However, the fit to our point spread function is not satisfactory, since it has an enhanced wing part at the spread angles from 3'' to 30'' which cannot be described by Fried's seeing function.

Figure 5 shows the blurring part of the point-spread function and its Fourier modulus (modulation transfer function, MTF). It is clear from Figure 5(b) that the MTF can be better fitted by a function of the form $\exp(-ak)$ than either the form of $\exp(-(ak)^2)$ (Gaussian) or $\exp(-(ak)^{5/3})$ (Fried's seeing function). The inverse Fourier transform of $\exp(-ak)$ is known to be a Moffat function of the form

$$\psi_{\text{bl}} = \frac{a}{2\pi(r^2 + a^2)^{3/2}} \quad (21)$$

as presented in Figure 5. The value of a which best fits the observed MTF presented in Figure 5 is found to be 2.2'', which corresponds to a full width at half maximum (FWHM) of 3.4''.

5.2. FROM THE INTENSITY POWER SPECTRUM

Figure 6 shows the observed power spectrum of the Stokes I image in Figure 2(a), and the modulation function of the blurring part of the point-spread function determined from the observed power spectrum. The intrinsic power spectrum shown in the figure has been adopted from the high-resolution observation of granulation

performed by Espagnet *et al.* (1993). The high-frequency tail of the power spectrum is more or less flat due to noise. We took 90% of the minimum value of the observed power for the noise power and subtracted it from the observed power to get noise-corrected power and MTF. As can be seen from Figure 6, the MTF is well described by a function of the form $\exp(-ak)$, which confirms the result we found in the MTF determined from the limb-intensity profile. The value of a is $1.5''$ in this case. This corresponds to a FWHM resolution of $2.3''$, which is smaller than $3.4''$ derived from Figure 1. This difference is qualitatively consistent with the fact that images in Figure 2 appear to have a higher contrast and show more detail than those in Figure 1.

6. Stray-Light Effect on Polarimetry

Measurements of polarizations are affected by both small and large-spread-angle stray light. Based on our results, we examine how each kind of stray-light influences polarization measurements.

We consider first the effect of large-spread-angle stray light. For simplicity, we neglect the effect of small-spread-angle stray light by assuming that ψ_{bl} is a δ -function. Then the equations presented in Section 2 yield

$$\frac{V^{obs}}{I^{obs}} = \frac{V}{I} \frac{(1 - \epsilon)I}{(1 - \epsilon)I + \epsilon S}. \quad (22)$$

This expression shows that the observed polarization degrees are always underestimated in the presence of large-spread-angle stray light and the underestimated factor depends on the intrinsic intensity I as well as the scattered-light fraction ϵ . As expected, the disturbance due to large spread-angle stray light is more serious in dark features than in bright features. For example, if we use $\epsilon = 0.15$ and $S = 1$, the value of observed polarization degree in a typical sunspot umbra with $I = 0.2$ would be only 53% of the undisturbed value, whereas the observed polarization degree of a feature with no contrast ($I = 1$) would be reduced by 15%, which is equal to ϵ .

Next, we examine the effect of small-spread-angle stray light. It is known that the the effect of small-spread-angle stray light on the measurement of polarization in a magnetic element is determined by the ratio of the feature size to the blurring size (Wang *et al.*, 1995; Lee *et al.*, 1997). Often both the magnetic element flux distribution and the blurring function are assumed to have Gaussian shapes. But we have found that the blurring part of the point spread function is better described by a Moffat function whose Fourier transform is given by an exponential function. Therefore, it will be interesting to examine the consequence of this specific functional form of the point spread function. For a simple illustration, we consider a magnetic element which has no intensity contrast ($I = 1$) and where spatial distribution of V is given in the same functional form as in Equation (21):

$$V = V_p \frac{1}{(1 + r^2/s^2)^{3/2}}. \quad (23)$$

Then it follows that

$$V^{\text{obs}} = V_p^{\text{obs}} \frac{1}{(1 + r^2/(s + a)^2)^{3/2}}, \quad (24)$$

where the observed peak value is given by $V_p^{\text{obs}} = V_p s^2/(s + a)^2$. We see that $V_p^{\text{obs}}/V_p = 0.5$ when $s/a \simeq 2.4$. This means that when the FWHM resolution of the point spread function is, e.g., $3.0''$, those magnetic elements whose FWHM sizes are less than $7.2''$ are seriously affected by small-angle stray light. This result is different from what is expected when Gaussian shapes are assumed for both the magnetic feature and the point spread function. In the latter case, the ratio of V_p^{obs} to V_p is given by $s^2/(s^2 + a^2)$, which implies that only magnetic features whose sizes are smaller than the blurring size are severely affected by small-spread-angle stray light.

7. Summary and Concluding Remarks

We have determined the point-spread functions of magnetograph observations using two indirect methods. The method using the limb-intensity profile turns out useful in determining the point spread functions in the wide range of spread angles including both the blurring part and the scattering part. The method using the photospheric intensity power spectrum is much simpler to use, but cannot give reliable information on the scattering part. It is found that the vector magnetograph observations typically have a scattered-light fraction of 0.15 (15%) and a FWHM spatial resolution of $3''$ on clear days.

We found from the two independent methods that the blurring part of the point-spread function is well described by a Moffat function whose Fourier transform is given by an exponential function. This supports the validity of the methods we use to derive the point-spread function. We do not understand why the point-spread function of magnetograph observations should be the Moffat function, unlike night-time observations. We suspect that either the scattering by thick calcite and quartz elements in the birefringent filter or the image motion during the integrations might produce stray light with spread angle between $3''$ and $30''$, which is well described by the Moffat function.

Our analysis shows that measurements of polarization in dark magnetic features like sunspots may be significantly underestimated due to the existence of large-spread-angle stray light. The polarization in darker sunspot umbral regions may be underestimated even by a factor of 50%. We also found that measurements of polarization in magnetic features of size smaller than $7''$ may be severely affected by small-spread-angle stray light. Thus it appears that both the large-spread-angle

and small-spread-angle stray light is a crucial problem in solar polarimetry. Figure 2 presents an example to illustrate this problem. The preceding main sunspot has many small satellite sunspots of opposite polarity which are very close to it. The measurements of polarization in these satellite sunspots must be affected by the polarized stray light originating from the main spot. Thus proper corrections of both kinds of stray light seem essential for making the best use of magnetogram data. The effect of large-spread-angle stray light can be corrected with ease only if the scattered light fraction ϵ is known. However, the correction for small-spread-angle stray light is not a trivial problem, because its effect depends on not only the point-spread function, but also the intrinsic spatial distribution of magnetic flux. The correction can be made only by solving the inversion problems given by Equations (7) and (8). We describe how to correct for stray light in magnetograph observations in the companion paper (Chae *et al.*, 1998).

Acknowledgements

We are grateful to Y. Nishino, K. Shinoda, and M. Noguchi for their support during the observations. One of us (J. Chae) would like to express his sincere thanks to T. Sakurai, K. Ichimoto, and Y. Suematsu for their hospitality given to him during his stay at Mitaka. We thank Martin Woodard and Carsten Denker for careful manuscript reading and good comments. The present work is supported in part by the Basic Research Institute Program, Ministry of Education, ROK, 1997 (BSRI-97-5408) and in part by the Korea-China Cooperative Science Program (966-0203-6056). This work is partially supported by NSF under grant ATM-9628862 and NASA under grant NAG5-3536 to BBSO.

References

- Albregtsen, F. and Andersen, B. N.: 1985, *Solar Phys.* **95**, 239.
Andersen, B. N.: 1986, *Solar Phys.* **107**, 27.
Brahde, R.: 1972, *Solar Phys.* **26**, 318.
Brault, J. W. and White, O. R.: 1971, *Astron. Astrophys.* **13**, 169.
Brown, T. M.: 1982, *Astron. Astrophys.* **116**, 260.
Chae, J., Yun, H. S., Sakurai, T., and Ichimoto, K.: 1998, *Solar Phys.* **183**, 245 (this issue).
Espagnet, O., Muller, R., Roudier, T., and Mein, N.: 1993, *Astron. Astrophys.* **271**, 589.
Fried, D. L.: 1966, *J. Opt. Soc. Am.* **16**, 1372.
Hansen, T.: 1973, *Solar Phys.* **32**, 505.
Keller, C. U.: 1991, in November, L. J. (ed.), *Solar Polarimetry*, National Solar Observatory, Sacramento Peak, p. 124.
Keller, C. U. and von der Lühe, O.: 1992, *Astron. Astrophys.* **261**, 321.
Koutchmy, S.: 1991, in November, L. J. (ed.), *Solar Polarimetry*, National Solar Observatory, Sacramento Peak, p. 237.
King, I. R.: 1971, *Publ. Astron. Soc. Pacific* **83**, 199.
Kneer, F. K. and Mattig, W.: 1968, *Solar Phys.* **5**, 42.

- Lawrence, J. K., Chapman, G. A., Herzog, A. D., and Shelton, J. C.: 1985, *Astrophys. J.* **292**, 297.
- Lee, J., Chae, J., Yun, H. S., and Zirin, H.: 1997, *Solar Phys.* **171**, 35.
- Lites, B. W. *et al.*: 1991, in November, L. (ed.), *Solar Polarimetry*, National Solar Observatory, Sacramento Peak, p. 3.
- Lites, B. W., Elmore, D. F., Seagraves, P., and Skumanich, A. P.: 1993, *Astrophys. J.* **418**, 928.
- Lites, B. W., Martínez Pillet, V., and Skumanich, A.: 1994, *Solar Phys.* **155**, 1.
- Maltby, P.: 1971, *Solar Phys.* **18**, 3.
- Martínez Pillet, V.: 1992, *Solar Phys.* **140**, 207.
- Mykland, N.: 1973, *Solar Phys.* **28**, 49.
- Pierce, A. K. and Slaughter, C. D.: 1977, *Solar Phys.* **51**, 25.
- Press, W. H., Flannery, B. P., Teukolsky, S. A., and Vetterling, W.T.: 1986, *Numerical Recipes*, Cambridge University Press, Cambridge.
- Rossbach, M. and Schröter, E. H.: 1970, *Solar Phys.* **12**, 95.
- Sakurai, T. *et al.*: 1995, *Publ. Astron. Soc. Japan* **47**, 81.
- Toner, C. G. and Jefferies, S. M.: 1993, *Astrophys. J.* **415**, 852.
- Wang, J., Wang, H., Tang, F., Lee, J., and Zirin, H.: 1995, *Solar Phys.* **160**, 277.
- Wittmann, A. and Wöhl, H.: 1975, *Solar Phys.* **44**, 231.